# Triplet fusion upconversion nanocapsules for volumetric 3D printing

https://doi.org/10.1038/s41586-022-04485-8

Received: 27 March 2020

Accepted: 28 January 2022

Published online: 20 April 2022



Check for updates

Samuel N. Sanders<sup>1,3</sup>, Tracy H. Schloemer<sup>1,2,3</sup>, Mahesh K. Gangishetty<sup>1</sup>, Daniel Anderson<sup>1</sup>, Michael Seitz<sup>1,2</sup>, Arynn O. Gallegos<sup>2</sup>, R. Christopher Stokes<sup>1</sup> & Daniel N. Congreve<sup>1,2 ⋈</sup>

Three-dimensional (3D) printing has exploded in interest as new technologies have opened up a multitude of applications<sup>1-6</sup>, with stereolithography a particularly successful approach<sup>4,7-9</sup>. However, owing to the linear absorption of light, this technique requires photopolymerization to occur at the surface of the printing volume, imparting fundamental limitations on resin choice and shape gamut. One promising way to circumvent this interfacial paradigm is to move beyond linear processes, with many groups using two-photon absorption to print in a truly volumetric fashion<sup>3,7-9</sup>. Using two-photon absorption, many groups and companies have been able to create remarkable nanoscale structures<sup>4,5</sup>, but the laser power required to drive this process has limited print size and speed, preventing widespread application beyond the nanoscale. Here we use triplet fusion upconversion<sup>10-13</sup> to print volumetrically with less than 4 milliwatt continuous-wave excitation. Upconversion is introduced to the resin by means of encapsulation with a silica shell and solubilizing ligands. We further introduce an excitonic strategy to systematically control the upconversion threshold to support either monovoxel or parallelized printing schemes, printing at power densities several orders of magnitude lower than the power densities required for two-photon-based 3D printing.

We demonstrate the advantage of a quadratic process (Fig. 1a, b), showing upconversion at the focal point of the excitation beam. This upconversion process takes advantage of excitonic states in annihilator molecules to generate an anti-Stokes emission relative to the absorption of the sensitizer; see Fig. 1c for a full description of the process. Crucially, the final upconversion step requires collisions of two excited annihilator triplets, which fuse to form one higher-energy annihilator singlet, which then emits blue light that can be used to locally drive photopolymerization by coupling with a photoinitiator. This process has a quadratic nature owing to the requirement for two triplets to meet, yet relatively low light fluences are required owing to the high absorption coefficient of the sensitizer as compared with two-photon absorption (2PA) because this process does not require simultaneous absorption of two photons by one molecule. Triplet fusion upconversion is also easily tunable in both excitation and emission wavelengths with judicious selection of the sensitizer and annihilator<sup>10</sup>.

When we initially attempted to use triplet fusion upconversion to drive 3D printing, we encountered several challenges. First, upconversion exhibits a threshold behaviour: the upconversion light intensity crosses over from a quadratic to a linear dependence on input light above a certain fluence. Achieving control over this threshold value is crucial to applying upconversion to different printing schemes. For example, for a single-voxel printing approach, we targeted a focal point with a power density on the order of >100 W cm<sup>-2</sup>. Although this operating power is much smaller than the  $10^{12}$  W cm<sup>-2</sup> required for 2PA, it is considerably higher than the threshold value for typical upconversion systems 10,14,15. On the other hand, using upconversion materials with a relatively low threshold would allow for low-fluence, rapid parallelized printing. Consequently, we needed systematic control over the threshold behaviour of the upconversion materials.

Further, because triplet fusion upconversion relies on high concentrations of strongly absorbing molecules undergoing frequent collisions, direct addition of the sensitizer and annihilator to the resin posed severe practical restrictions. High concentrations of the molecules would need to be dissolved in the 3D printing resin, resulting in excessive attenuation of the input light and limited print volumes  $^{16,17}$ . Further, as the resin viscosity increases during printing, the rate of molecular collisions decreases, reducing the upconversion efficiency and resulting in a loss of the print selectivity. Taken together, we needed to engineer a sensitizer and annihilator pair such that we could access a wide range of upconversion threshold values, while simultaneously deploying them in a way to ensure both a high local concentration to maximize upconversion efficiency and a low global concentration of the upconversion materials to maximize light-penetration depths.

To tackle these challenges, we first developed a strategy to tune the  $upconversion\,threshold.\,We\,selected\,9,10\text{-}bis((triisopropylsilyl)ethy-conversion\,threshold)$ nyl)anthracene (TIPS-anthracene) as the annihilator and palladium(II) -meso-tetraphenyl-tetrabenzoporphyrin (PdTPTBP) as the sensitizer (Fig. 2a). This red-to-blue upconversion system works with favourable  $reported\,efficiencies\,of\,up\,to\,30\% (ref.\,{}^{14}).\,However, the\,TIPS-anthracene$ 

Rowland Institute at Harvard University, Cambridge, MA, USA. 2Department of Electrical Engineering, Stanford University, Stanford, CA, USA. 3These authors contributed equally: Samuel N. Sanders, Tracy H. Schloemer. <sup>™</sup>e-mail: congreve@stanford.edu

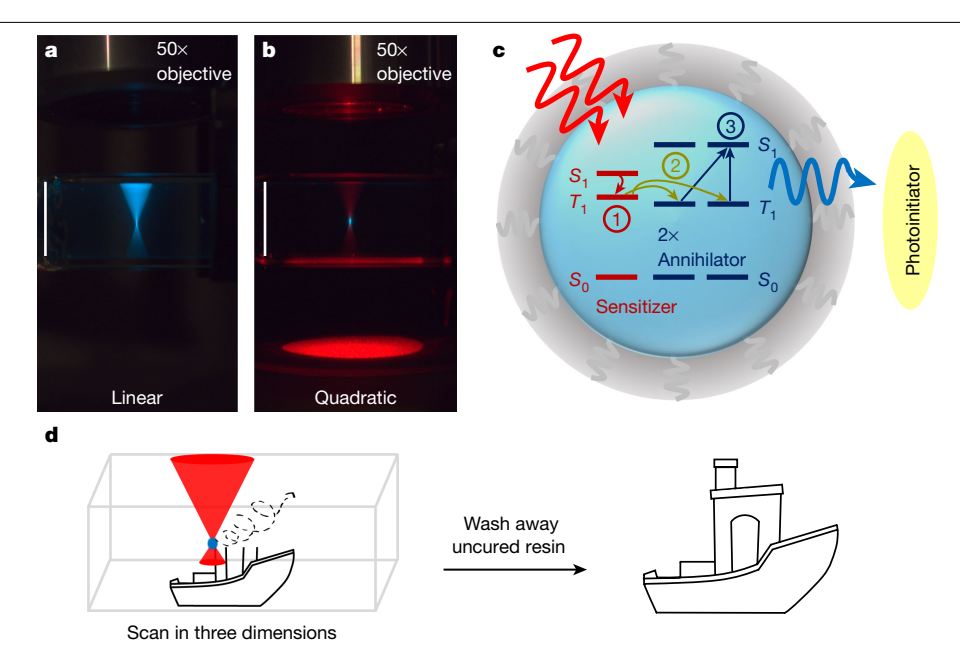


Fig.1 | Triplet fusion upconversion for 3D printing. a, b, Comparison between $linear and \, quadratic \, absorption \, processes \, in \, a \, 1\text{-cm} \, cuvette \, of \, PdTPTBP \, and \, respectively. \, and \, respectively in the processes in \, a \, 1\text{-cm} \, cuvette \, of \, PdTPTBP \, and \, respectively. \, and \, respectively in the processes in \, a \, 1\text{-cm} \, cuvette \, of \, PdTPTBP \, and \, respectively. \, An example of \, PdTPTBP \, and \, respectively$ Br-TIPS-anthracene in oleic acid. The linear process results from directly exciting the annihilator at 365 nm. As a result, blue light is generated throughout the cuvette and visibly attenuates as a function of depth. The quadratic process results from triplet fusion upconversion by exciting the sensitizer at 637 nm, and blue light is generated only at the focal spot. The scale bars denote  $1\,\mathrm{cm}$ .  $\mathbf{c}$ , A cartoon

depiction of the upconversion process occurring in the oleic acid core of a UCNC.Two low-energy photons generate two singlet excitons on sensitizer molecules, which intersystem cross (1) to generate triplet excitons. These excitons then triplet energy transfer to the annihilator (2), where they undergo triplet fusion (3) to generate a higher energy singlet, which can radiatively decay by emitting a  $high-energy\,photon\,that\,is\,absorbed\,by\,the\,photoinitiator.\,\textbf{d}, Cartoon\,depiction\,of$  $the \, UCNC \hbox{-} facilitated \, printing \, process \, using \, monovoxel \, excitation.$ 

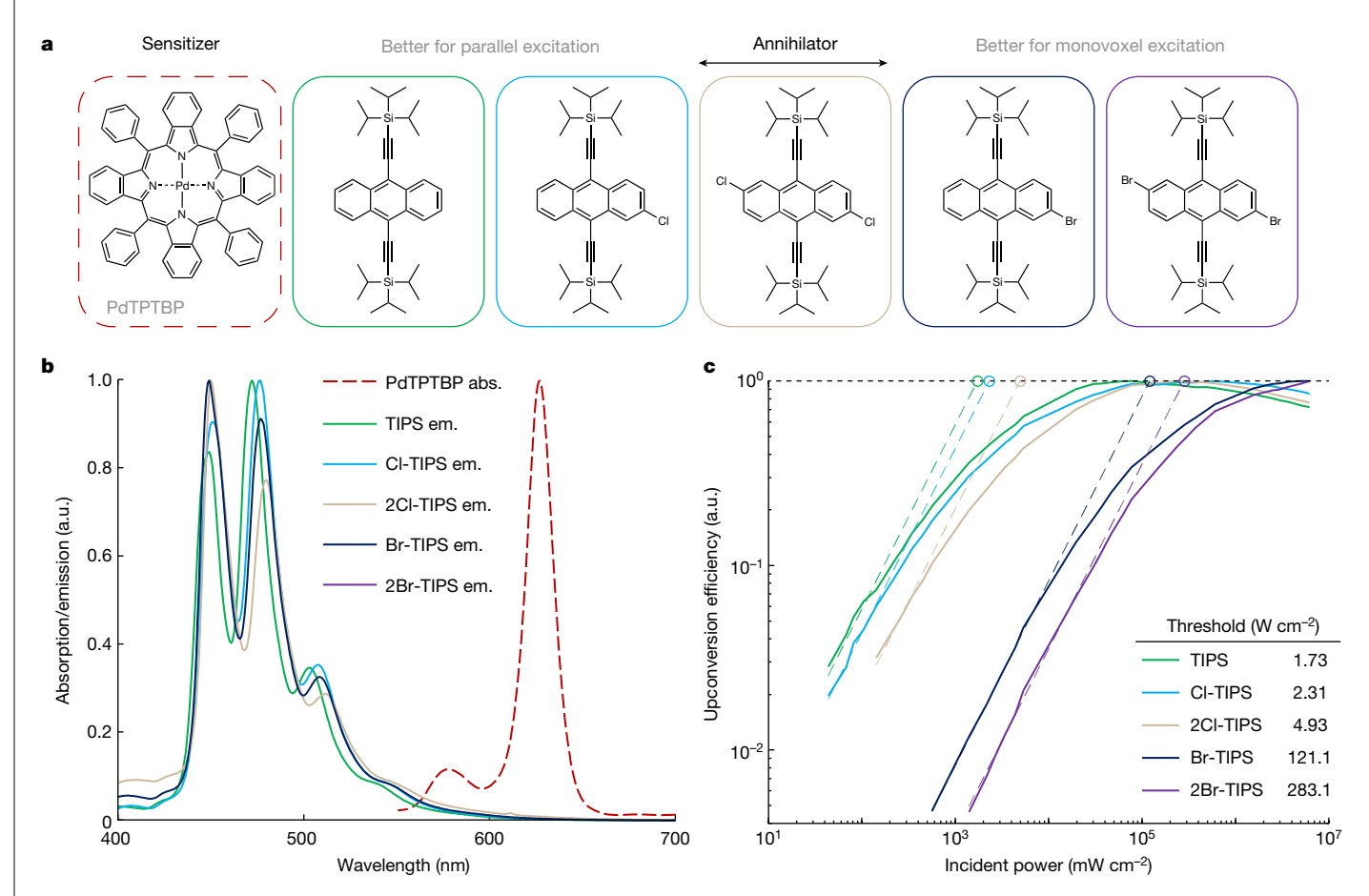
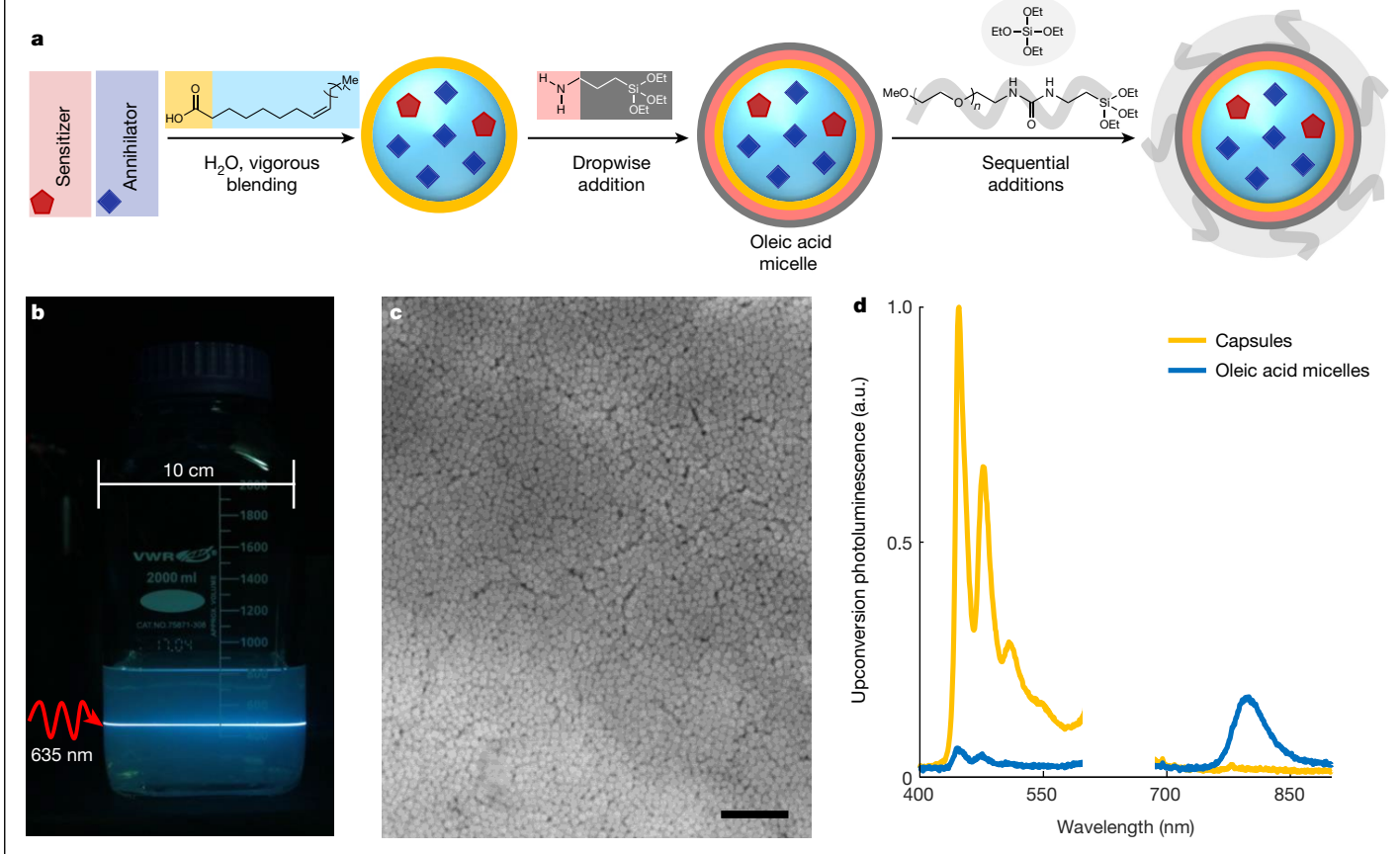


Fig. 2 | Tuning the upconversion threshold. a, From left to right, the chemical structures of PdTPTBP, TIPS-anthracene, Cl-TIPS-anthracene, 2CI-TIPS-anthracene, Br-TIPS-anthracene and 2Br-TIPS-anthracene. **b**, The Q band absorption of the sensitizer, PdTPTBP (dashed red line), and the

photoluminescence of the annihilators.  ${f c}$ , The upconversion efficiency as a function of input power. The intersection of a linear fit (dashed lines) to the quadratic regime and the maximum efficiency of the linear regime gives the threshold of each material (circles), summarized in the inset table.



**Fig. 3** | **Durable encapsulation of upconversion materials. a**, Overview of the UCNC synthesis. Oleic acid nanodroplet micelles containing upconversion materials are encapsulated in silica and further decorated with covalently bound PEG chains. **b**, UCNCs diluted in acetone show long light-penetration depths. The capsules are excited at 635 nm and are imaged through a 550-nm short-pass filter. **c**, SEM image of the UCNCs shows the scale and uniformity of

the nanoparticle synthesis. The scale bar denotes  $500\,\mathrm{nm}$ . **d**, Dispersion of the oleic acid micelles (blue) and final UCNCs (orange) in acetone under  $635\,\mathrm{nm}$  excitation shows the necessity of the silica shell to upconversion survival. The emission peak at about  $800\,\mathrm{nm}$  corresponds to phosphorescence from the sensitizer PdTPTBP.

threshold of 1.7 W cm<sup>-2</sup> was far too low to power our single-voxel printer. The threshold value of a triplet fusion system can be related to the non-radiative triplet decay rate  $k_{\rm A}$  and the rate of triplet fusion  $k_{\rm TF}$  (refs. <sup>18,19</sup>):

$$I_{\text{Threshold}} \propto \frac{k_{\text{A}}^2}{k_{\text{TF}}}$$

To increase the threshold, we focused on increasing the triplet recombination rate,  $k_A$ , by adding heavy atoms to the molecule and subsequently increasing the threshold value,  $I_{\text{Threshold}}$  (ref. <sup>20</sup>). We synthesized a series of acenes with heavy-atom substitution to adjust the threshold; see Fig. 2a and Methods<sup>21</sup>. The introduction of halogens to the anthracene core introduces little difference in emission or absorbance, yet the upconversion thresholds vary tremendously with the simple changes in the annihilator; see Fig. 2 and Extended Data Fig. 1. In Fig. 2c, we plot the relative upconversion efficiency of each of these acenes against power density. The relative efficiency increases at low powers until the threshold, at which it plateaus and becomes constant. Notably, the measured thresholds range from 1.7 W cm<sup>-2</sup> for unsubstituted TIPS-anthracene all the way up to 283 W cm<sup>-2</sup> for the 2Br-TIPS-anthracene, spanning more than two orders of magnitude. This molecular library imparts enormous flexibility in printer design: a monovoxel excitation source can take advantage of the high threshold of Br-TIPS-anthracene or 2Br-TIPS-anthracene annihilators, whereas a large-area parallel excitation printer, which requires lower excitation intensities to drive thousands of voxels simultaneously, could use the CI-TIPS-anthracene or even the unsubstituted TIPS-anthracene annihilators (Extended Data Fig. 2).

With the upconversion materials in hand, we turned to the challenge of their deployment. To achieve this, we sought to encapsulate nanodroplets of the upconversion stock solutions to maintain a high local concentration of materials. We targeted nanoscale dimensions to minimize the optical scatter of the printing resin. Although we and others have previously built upconverting micelles out of block copolymers for applications in aqueous solutions, we found that these micelles were unstable in organic solvents<sup>22-25</sup>. Instead, we sought a nanoencapsulation that would disperse in organic-solvent-based 3D printing resins without leaking the contents or scattering light. We were inspired by recent work from Kwon et al.<sup>22</sup>, who built substantially more durable upconverting silica nanocapsules relative to previous reports<sup>23–25</sup>. Even so, we found that these materials notably scattered the input laser beam, owing to aggregation of the nanocapsules (Extended Data Fig. 1). To overcome these challenges, we designed a nanocapsule synthesis that incorporated a long poly(ethylene glycol) (PEG) chain as a solubilizing ligand on the exterior of the silica shell. Incorporating a silane-terminated PEG that can covalently graft to the silica shell of the nanocapsule<sup>26</sup> was crucial to prevent aggregation over time and to allow the nanocapsules to disperse without scatter in 3D printing resins (Fig. 3b, Extended Data Fig. 1). Full details of the optimized nanocapsule synthesis can be found in Fig. 3a and Methods.

Electron microscopy of the resulting upconversion nanocapsules (UCNCs) shows uniform capsule sizes of approximately 50 nm in

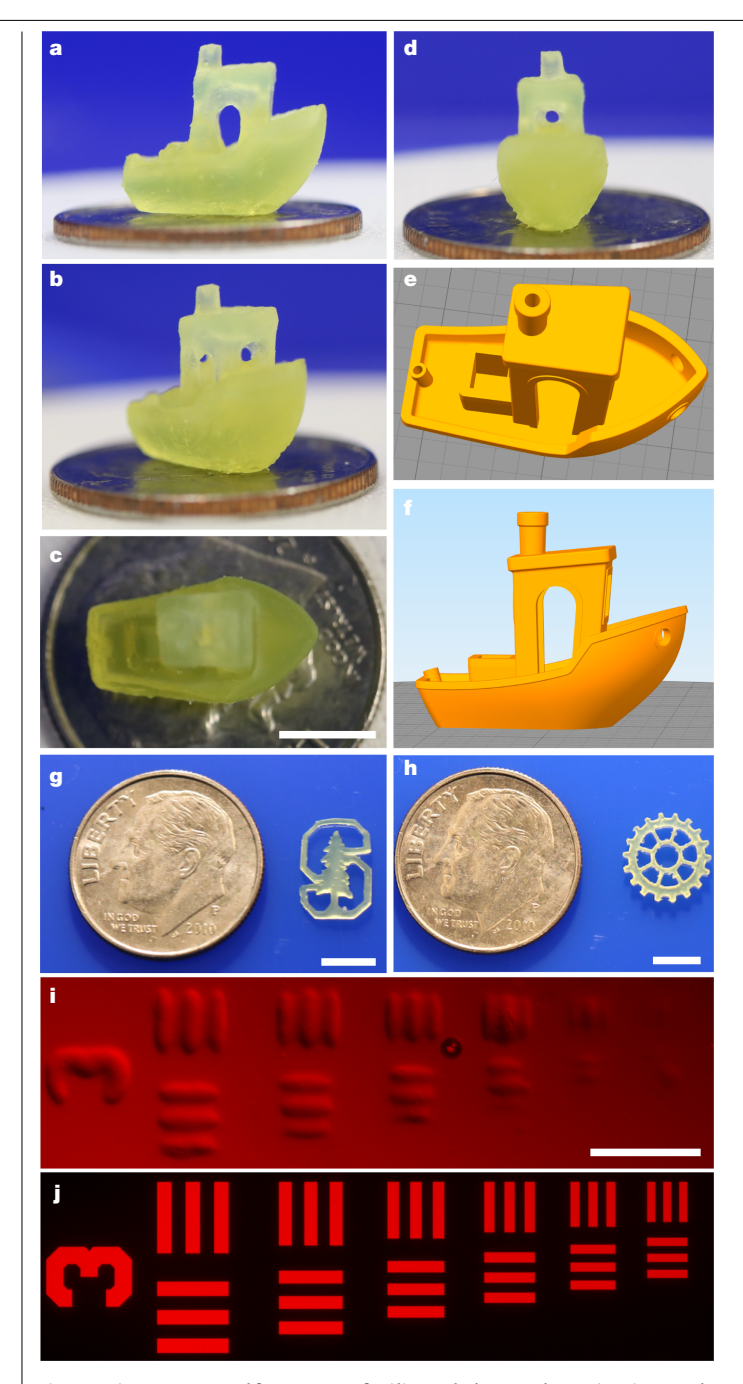


Fig. 4 | Prints generated from UCNC-facilitated photopolymerization. a-d, Side and top views of our final benchmark boat (Benchy) print cured using monovoxel excitation printing, sitting on a dime for scale. The scale bar denotes 5 mm. e, f, Top and side views of the Benchy STL file. The side and top views of the final print show the faithful reproduction of the main features. g, h, Top views of the Stanford logo (g) and gear (h) prints cured using large-area, two-dimensional parallel excitation printing, sitting next to a dime for scale. The scale bars denote 5 mm. i, j, Microscope images of lines printed in about 0.1 ml of resin (i) with light projected through the United States Air Force Target Test mask (j). The scale bar denotes 500 μm.

diameter (Fig. 3c, Extended Data Fig. 1) and dynamic light scattering shows good batch-to-batch consistency (Extended Data Table 1). Of particular importance is the stability imparted by the silica shell. To demonstrate this, we diluted the nanocapsule solution from both the initial micelle formation after dropwise addition of (3-aminopropyl) triethoxysilane (APTES) and the final shelled UCNCs at 100:1 in acetone.

In the former case, the micelles fall apart, resulting in limited upconversion and notable PdTPTBP phosphorescence at about 800 nm. In the latter case, the bright upconversion from the UCNCs is preserved with minimal sensitizer phosphorescence (Fig. 3d). In addition to the durability improvements, we highlight the negligible phosphorescence observed in the UCNCs, which is extremely challenging to suppress in encapsulated systems<sup>24</sup> and signifies efficient collisions between sensitizer and annihilator. We were further able to disperse the capsules in several common solvents while maintaining bright upconversion (see Extended Data Fig. 1).

We then introduced our capsules to a simple 3D printing resin consisting of all commercially available materials; the full fabrication details are presented in Methods. First, acrylic acid was selected to disperse the nanocapsules in an acrylate-based monomer. We then used pentaerythritol tetraacrylate (PETA) to introduce the capsules into a highly cross-linkable matrix. The commercially available photoinitiator Ivocerin (bis(4-methoxybenzoyl)diethylgermanium) was used to absorb the blue upconversion emission and initiate the free radical polymerization (Extended Data Fig. 1). The addition of a radical inhibitor, 2,2,6,6-tetra methylpiperidin-1-yl)oxyl (TEMPO) at 3 ppm improves the print resolution by efficiently terminating carbon-carbon radicals [7, 27], preventing notable polymerization outside the irradiated voxel. We also added a broad-spectrum light blocker, 1-phenylazo-2-naphthol (Sudan I; refs. <sup>28,29</sup>), to sharpen the resolution by attenuating the upconverted light outside the focal point (Extended Data Fig. 1). Finally, the resin viscosity is further increased with the addition of a hydrophilic fused silica to generate self-supporting prints (Aerosil 200, see Supplementary Video 1).

For monovoxel printing, by overfilling the back aperture of a 0.55-NA objective with a collimated laser beam and mounting the objective onto a fused deposition modelling (FDM) printer, we were able to trace a well-defined focal point in space throughout resins using Br-TIPS-anthracene as the nanoencapsulated annihilator (Fig. 1d, Extended Data Fig. 2, Supplementary Video 2). Owing to the quadratic power dependence of triplet fusion, the upconversion is active predominantly at the focal point of the laser, resulting in a confined blue voxel that drives local photopolymerization.

A standard yet difficult test of 3D printing systems is the benchmark boat print (often referred to as Benchy<sup>30</sup>), shown in Fig. 4a-f and Extended Data Fig. 3. In a proof of concept for printing with this technology, we faithfully reproduce this print at small scales using the monovoxel printing setup and the optimized Br-TIPS-anthracene-based resin. Printing without support structures simplifies post-processing and limits surface blemishes; see Extended Data Fig. 3 to compare with the same file simulated on a commercial printer in which >80% of the resin is used in the support structure. The power and print speed were carefully optimized to prevent 'underprinting' and 'overprinting' (Extended Data Fig. 3) to realize high-fidelity, reproducible prints in under 2 h (Fig. 4a-f, Extended Data Fig. 3, Extended Data Table 2). We print at power densities of 4.5 × 10<sup>3</sup> – 4.9 × 10<sup>3</sup> W cm<sup>-2</sup> (Extended Data Fig. 2, Supplementary Video 2), confining linear upconversion to within approximately 80 µm from the focal point of the voxel (Extended Data Fig. 4). We further exemplify the fine detail attainable by printing the Harvard University logo (Extended Data Fig. 3, Supplementary Video 3).

We also demonstrate large-area, two-dimensional parallel excitation printing to generate an intricate gear using the lowupconversion-threshold TIPS-anthracene-based resin as a proof of concept (Extended Data Fig. 2, Supplementary Video 4). We print a detailed gear and a Stanford University logo in 8 min at 78 mW cm<sup>-2</sup> using a light-emitting diode (LED) light source patterned by a digital micromirror device (DMD) printer (Fig. 4g-j, Extended Data Fig. 3). We present the full print and washing process in Supplementary Video 4. Microscope images show minimal surface blemishes on the gear, even after the excess resin was washed away (Extended Data Fig. 3).

We then sought to quantify the smallest features attainable with our optimized resin using the DMD projection system and a mask to pattern lines; see Methods. We reproducibly printed features as small

as 50 µm (Fig. 4i, j, Extended Data Table 3). We anticipate that smaller features could be generated with a combination of improved optics and resin formulation (Extended Data Fig. 5, Extended Data Table 4).

In summary, by using a process with a quadratic dependence on light intensity and low-threshold nanocapsules, we demonstrate the ability to arbitrarily pattern light and cure considerable volumes of resin compared with other quadratic processes. There is critical need for advancing the processing speed of volumetric printing to deliver intricate resolution prints in practical timescales<sup>31</sup>. Although the optical and algorithmic engineering required to achieve 3D selectivity with multi-voxel printing is beyond the scope of the current work, we demonstrate curing of considerable volumes of resin in minutes instead of tens of hours required using 2PA-based printing<sup>31-33</sup>. Further, our approach can print with lower-energy laser inputs and with higher speeds compared with 2PA. Although there are reports of photopolymerization using upconverted light<sup>11,34-43</sup> (Extended Data Table 5), the threshold tuning across a wide range of power densities, the shape gamut versatility and the range of power densities used are unique to this work. We expect that the ability to tune the UCNC threshold behaviour over orders of magnitude will be applicable to a variety of printing excitation schemes beyond the simple monovoxel or parallel excitation printers demonstrated here, such as full, projector-based printing approaches for a variety of applications that require rapid, customizable, precision 3D printing. Finally, we expect to combine this technique with recent technological developments in optical parallelization to greatly increase print speeds<sup>44-46</sup>. The ability to simply exchange the UCNC contents is a critical feature that enables discrete, localized photochemistry for many applications within the realm of 3D printing. We believe that UCNCs can serve as a key enabling technology for a variety of optically controlled systems that currently suffer from high-energy light-penetration limitations.

## Online content

Any methods, additional references, Nature Research reporting summaries, source data, extended data, supplementary information, acknowledgements, peer review information; details of author contributions and competing interests; and statements of data and code availability are available at https://doi.org/10.1038/s41586-022-04485-8.

- MacDonald, E. & Wicker, R. Multiprocess 3D printing for increasing component functionality, Science 353, aaf2093 (2016)
- 2. Gladman, A. S., Matsumoto, E. A., Nuzzo, R. G., Mahadevan, L. & Lewis, J. A. Biomimetic 4D printing. Nat. Mater. 15, 413-418 (2016).
- Anscombe, N. Direct laser writing. Nat. Photon. 4, 22-23 (2010).
- Geng, Q., Wang, D., Chen, P. & Chen, S.-C. Ultrafast multi-focus 3-D nano-fabrication based on two-photon polymerization. Nat. Commun. 10, 2179 (2019).
- 5. Cumpston, B. H. et al. Two-photon polymerization initiators for three-dimensional optical data storage and microfabrication. Nature 398, 51-54 (1999).
- 6. Hong, S, et al. 3D printing of highly stretchable and tough hydrogels into complex. cellularized structures, Adv. Mater. 27, 4035-4040 (2015).
- Ligon, S. C., Liska, R., Stampfl, J., Gurr, M. & Mülhaupt, R. Polymers for 3D printing and 7. customized additive manufacturing. Chem. Rev. 117, 10212-10290 (2017).
- 8. Xiong, W. et al. Simultaneous additive and subtractive three-dimensional nanofabrication using integrated two-photon polymerization and multiphoton ablation. Light: Sci. Appl. 1, e6 (2012).
- 9 LaFratta, C. N. & Li, L. in Three-Dimensional Microfabrication Using Two-Photon Polymerization (ed. Baldacchini, T.) 221-241 (Elsevier, 2016).
- Singh-Rachford, T. N. & Castellano, F. N. Photon upconversion based on sensitized triplettriplet annihilation. Coord. Chem. Rev. 254, 2560-2573 (2010).
- 11. Ravetz, B. D. et al. Photoredox catalysis using infrared light via triplet fusion upconversion. Nature 565, 343-346 (2019).
- Mongin, C., Garakyaraghi, S., Razgoniaeva, N., Zamkov, M. & Castellano, F. N. Direct observation of triplet energy transfer from semiconductor nanocrystals. Science 351, 369-372 (2016).
- Schmidt, T. W. & Castellano, F. N. Photochemical upconversion: the primacy of kinetics. J. Phys. Chem. Lett. 5, 4062-4072 (2014).
- Nishimura, N. et al. Photon upconversion from near-infrared to blue light with TIPS-anthracene as an efficient triplet-triplet annihilator. ACS Mater. Lett. 1, 660-664
- Meinardi, F. et al. Quasi-thresholdless photon upconversion in metal-organic framework nanocrystals. Nano Lett. 19, 2169-2177 (2019).

- Awwad, N., Bui, A. T., Danilov, F. O. & Castellano, F. N. Visible-light-initiated free-radical polymerization by homomolecular triplet-triplet annihilation. Chem 6, 3071-3085 (2020).
- Limberg, D., Kang, J.-H. & Hayward, R. Triplet-triplet annihilation polymerization (TTAP) for high resolution 3D printing. American Physical Society Meeting Vol. 66 abstract C08.00009 (2021)
- Dzebo, D., Börjesson, K., Gray, V., Moth-Poulsen, K. & Albinsson, B. Intramolecular triplettriplet annihilation upconversion in 9,10-diphenylanthracene oligomers and dendrimers. J. Phys. Chem. C 120, 23397-23406 (2016).
- Monguzzi, A., Mezyk, J., Scotognella, F., Tubino, R. & Meinardi, F. Upconversion-induced fluorescence in multicomponent systems: steady-state excitation power threshold. Phys. Rev. B 78, 195112 (2008).
- McGlynn, S. P., Reynolds, M. J., Daigre, G. W. & Christodoyleas, N. D. The external heavy-atom spin-orbital coupling effect. III. Phosphorescence spectra and lifetimes of externally perturbed naphthalenes. J. Phys. Chem. 66, 2499-2505 (1962).
- Chung, D. S. et al. High mobility organic single crystal transistors based on soluble triisopropylsilylethynyl anthracene derivatives. J. Mater. Chem. 20, 524-530 (2009).
- Kwon, O. S., Kim, J.-H., Cho, J. K. & Kim, J.-H. Triplet-triplet annihilation upconversion in CdS-decorated SiO<sub>2</sub> nanocapsules for sub-bandgap photocatalysis. ACS Appl. Mater. Interfaces 7, 318-325 (2015).
- Liu, Q., Yang, T., Feng, W. & Li, F. Blue-emissive upconversion nanoparticles for low-power-excited bioimaging in vivo. J. Am. Chem. Soc. 134, 5390-5397 (2012).
- Sanders, S. N., Gangishetty, M. K., Sfeir, M. Y. & Congreve, D. N. Photon upconversion in aqueous nanodroplets. J. Am. Chem. Soc. 141, 9180-9184 (2019).
- 25. Liu, Q. et al. Highly photostable near-IR-excitation upconversion nanocapsules based on triplet-triplet annihilation for in vivo bioimaging application. ACS Appl. Mater. Interfaces 10, 9883-9888 (2018).
- Jo, S. & Park, K. Surface modification using silanated poly(ethylene glycol)s. Biomaterials **21**, 605-616 (2000).
- Ma, Y. Nitroxides in Mechanistic Studies: Ageing of Gold Nanoparticles and Nitroxide Transformation in Acids Ch. 3, PhD thesis, Univ. York (2010).
- Gong, H., Beauchamp, M., Perry, S., Woolley, A. T. & Nordin, G. P. Optical approach to resin formulation for 3D printed microfluidics. RSC Adv. 5, 106621-106632 (2015).
- Ahn, D., Stevens, L. M., Zhou, K. & Page, Z. A. Rapid high-resolution visible light 3D printing. ACS Cent. Sci. 6, 1555-1563 (2020).
- Thingiverse.com. #3DBenchy the jolly 3D printing torture-test by CreativeTools.se by CreativeTools; https://www.3dbenchy.com
- 31. Matheu, M., Busby, E. & Borglin, J. Human organ and tissue engineering: advances and challenges in addressing the medical crisis of the 21st century https://www.semanticscholar. org/paper/Human-Organ-and-Tissue-Engineering-%3A-Advances-and-Matheu-Busby/5c187 83fcaOcd38708ad4933784bbdb9554111df (2018).
- 32. Chu, W. et al. Centimeter-height 3D printing with femtosecond laser two-photon polymerization, Adv. Mater. Technol. 3, 1700396 (2018).
- 33. Saha, S. K. et al. Scalable submicrometer additive manufacturing, Science 366, 105-109 (2019)
- Stepuk, A. et al. Use of NIR light and upconversion phosphors in light-curable polymers. 34. Dent Mater 28 304-311 (2012)
- Liu, R., Chen, H., Li, Z., Shi, F. & Liu, X. Extremely deep photopolymerization using upconversion particles as internal lamps. Polym. Chem. 7, 2457-2463 (2016).
- 36. Méndez-Ramos, J., Ruiz-Morales, J. C., Acosta-Mora, P. & Khaidukov, N. M. Infrared-light induced curing of photosensitive resins through photon up-conversion for novel cost-effective luminescent 3D-printing technology. J. Mater. Chem. C 4, 801-806 (2016).
- Sun, T. et al. Integrating temporal and spatial control of electronic transitions for bright multiphoton upconversion. Nat. Commun. 10, 1811 (2019).
- 38. Rocheva, V. V. et al. High-resolution 3D photopolymerization assisted by upconversion nanoparticles for rapid prototyping applications. Sci. Rep. 8, 3663 (2018).
- Chen, Z., He, S., Butt, H.-J. & Wu, S. Photon upconversion lithography: patterning of biomaterials using near-infrared light. Adv. Mater. 27, 2203-2206 (2015).
- Darani, M. K., Bastani, S., Ghahari, M., Kardar, P. & Mohajerani, E. NIR induced photopolymerization of acrylate-based composite containing upconversion particles as an internal miniaturized UV sources. Prog. Org. Coat. 104, 97-103 (2017).
- Liu, R., Zou, X., Xu, Y., Liu, X. & Li, Z. Deep thiol-ene photopolymerization using upconversion nanoparticle-assisted photochemistry. Chem. Lett. 45, 1054-1056 (2016)
- Demina, P. et al. Polymerization assisted by upconversion nanoparticles under NIR light. Molecules 24, 2476 (2019).
- Wang, Z. et al. Spatially confined photoexcitation with triplet-triplet annihilation 43. upconversion, Chem. Commun. 57, 9044-9047 (2021).
- Kellv. B. E. et al. Volumetric additive manufacturing via tomographic reconstruction. Science 363, 1075-1079 (2019).
- Loterie, D., Delrot, P. & Moser, C. High-resolution tomographic volumetric additive 45. manufacturing. Nat. Commun. 11, 852 (2020).
- 46 Regehly, M. et al. Xolography for linear volumetric 3D printing. Nature 588, 620-624 (2020)
- 47. Goto, K. et al. Intermolecular oxidative annulation of 2-aminoanthracenes to diazaacenes and aza[7]helicenes. Angew. Chem. Int. Ed. 51, 10333-10336 (2012).
- 48. Sanders, S. N. et al. Intramolecular singlet fission in oligoacene heterodimers. Angew. Chem. Int. Ed. 55, 3373-3377 (2016).
- Chung, D. S. et al. High mobility organic single crystal transistors based on soluble triisopropylsilylethynyl anthracene derivatives. J. Mater. Chem. 20, 524-530 (2010).
- Speckbacher, M., Yu, L. & Lindsey, J. S. Formation of porphyrins in the presence of acid-labile metalloporphyrins: a new route to mixed-metal multiporphyrin arrays. Inorg. Chem. 42, 4322-4337 (2003)

Publisher's note Springer Nature remains neutral with regard to jurisdictional claims in published maps and institutional affiliations.

© The Author(s), under exclusive licence to Springer Nature Limited 2022

#### Methods

#### **Materials**

All chemicals were used as received. (Triisopropylsilyl)acetylene, *n*-butyllithium (2.5M in hexanes), PETA, Sudan I, TEMPO, poly(ethylene glycol) diacrylate (PEGDA) and acrylic acid were purchased from Sigma-Aldrich. PdTPTBP was purchased from Frontier Scientific. 99% oleic acid was purchased from Beantown Chemical. Anhydrous tetraethyl orthosilicate (TEOS) and APTES were purchased from Acros Organics. 10K MPEG-Silane was purchased from Nanosoft Polymers. Ivocerin was purchased from Synthon Chemicals GmbH & Co. 2,6-dichloroanthracenequinone was purchased from HAARES ChemTech. Aerosil 200 was provided by Evonik Industries.

#### **Annihilator synthesis**

TIPS-anthracene was purchased commercially from Sigma-Aldrich. The bromo-TIPS-anthracene (2-bromo-9,10-bis[(triisopropylsilyl) ethynyl]anthracene) and dibromo-TIPS-anthracene (2,6-dibromo-9,10-bis[(triisopropylsilyl)ethynyl]anthracene) syntheses have been reported previously<sup>47-49</sup>. The chloro-TIPS-anthracene and dichloro-TIPS-anthracene were synthesized according to the same protocol.

**Chloro-TIPS-anthracene (2-chloro-9,10-bis[(triisopropylsilyl) ethynyl]anthracene).** To a solution of  $8.21\,\mathrm{ml}$  (36.6 mmol, 3.5 eq) of TIPS-acetylene in 10 ml of dry tetrahydrofuran in an inert atmosphere at 0 °C, 13.8 ml of  $2.5M\,n$ -butyllithium in hexanes (34.5 mmol, 3.3 eq) was added. This solution was kept at 0 °C for 30 min, then  $2.54\,\mathrm{g}$  (10.4 mmol, 1 eq) of 2-chloro, 9,10-anthracenequinone was added. The solution was allowed to warm to room temperature over the course of an hour, when  $6.00\,\mathrm{g}$  of  $\mathrm{SnCl_2}^*\mathrm{2H_2O}$  (26.6 mmol,  $2.6\,\mathrm{eq}$ ) was added, along with 1 ml of 10% aqueous hydrochloric acid, and the reaction was stirred for another hour. The resulting solution was extracted between hexanes and water three times and then solvent and residual TIPS-acetylene were removed in vacuo. Column chromatography on silica gel (hexanes and dichloromethane) yielded product as a bright yellow solid.

1.83 g (31% yield)

<sup>1</sup>H NMR (600 MHz, CDCl<sub>3</sub>, δ ppm): 8.66 (d,1H), 8.62 (m, 2H), 8.66–8.63 (m, 2H), 8.59 (d, 1H), 7.63 (m, 2H), 7.55 (m, 1H), 1.28 (m, 42H)

<sup>13</sup>C NMR (125 MHz, CDCl<sub>3</sub>, δ ppm): 135.80, 135.47, 135.45, 135.07, 133.25, 131.72, 130.62, 130.04, 129.97, 129.90, 129.76, 128.60, 121.65, 120.55, 108.24, 108.11, 105.50, 105.43, 21.53, 14.17, 14.15

MS (ESI): calculated m/z: 572.305; observed m/z: 572.3066

Dichloro-TIPS-anthracene (2,6-dichloro-9,10-bis[(triisopropylsil yl)ethynyl]anthracene). To a solution of  $8.21\,\mathrm{ml}$  (36.6 mmol, 3.5 eq) of TIPS-acetylene in 10 ml of dry tetrahydrofuran in an inert atmosphere at 0 °C, 13.8 ml of  $2.5M\,n$ -butyllithium in hexanes (34.5 mmol, 3.3 eq) was added. This solution was kept at 0 °C for 30 min, then  $2.90\,\mathrm{g}$  (10.4 mmol, 1 eq) of 2,6-dichloro, 9,10-anthracenequinone was added. The solution was allowed to warm to room temperature over the course of an hour, when  $6.00\,\mathrm{g}$  of  $\mathrm{SnCl_2}^*\mathrm{2H_2O}$  (26.6 mmol,  $2.6\,\mathrm{eq}$ ) was added, along with 1 ml of 10% aqueous hydrochloric acid, and the reaction was stirred for another hour. The resulting solution was extracted between hexanes and water three times, and then solvent and residual TIPS-acetylene were removed in vacuo. Column chromatography on silica gel (hexanes and dichloromethane) yielded product as a bright yellow solid.

2.14 g (34% yield)

 $^{1}$ H NMR (600 MHz, CDCl<sub>3</sub>,  $\delta$  ppm): 8.62 (d, 2H), 8.54 (d, 2H), 7.55 (m, 2H) 1.28 (m, 42H)

<sup>13</sup>C NMR (125 MHz, CDCl<sub>3</sub>, δ ppm): 136.13, 135.44, 133.60, 131.66, 131.20, 128.67, 120.84, 108.87, 104.92, 21.49, 14.13

MS (ESI): calculated *m/z*: 606.2666; observed *m/z*: 606.2676

#### **UCNC** synthesis

Fresh upconversion stock solutions were prepared for each batch of capsules. Under red lighting, saturated solutions of the sensitizer (PdTPTBP, 2 mg ml<sup>-1</sup>) and annihilator (TIPS-anthracene, 8 mg ml<sup>-1</sup>, or Br-TIPS-anthracene, 70 mg ml<sup>-1</sup>) were prepared in 99% oleic acid at room temperature, and the mixtures were allowed to stir for at least 4 h before filtering with a 0.45-µm polytetrafluoroethylene (PTFE) filter. These solutions were prepared under red lighting to prevent the demetallation of PdTPTBP in oleic acid<sup>50</sup>. Stock solutions for nanoencapsulation were prepared by mixing these solutions together along with extra, neat oleic acid. Stock solutions for TIPS-anthracene capsules were 2:1:2 TIPS-anthracene:PdTPTBP:oleic acid by volume and stock solutions for Br-TIPS-anthracene capsules were 0.5:1:3.5 Br-TIPS-anthracene:PdTPTBP:oleic acid by volume. After the stock solutions were prepared, rigorous red lighting was no longer required and ambient lighting was used. Milli-Q water (200 ml) was chilled over an ice bath for at least 1 h (temperature around 5 °C) and poured into to a Vitamix blender (Vitamix E310 Explorian Blender, Professional Grade, 48 oz, Amazon.com) in a nitrogen-filled glovebox. The upconversion stock solution containing the sensitizer and the annihilator (1.45 ml) was carefully dispensed into the water in one portion. The solution was blended for 60 s at the maximum speed, and the emulsion was transferred to a 500-ml, two-necked, round-bottom flask and immediately stirred at high speed with an egg-shaped stir bar (about 1,000 rpm). (3-aminopropyl)triethoxysilane (0.75 ml) was added until the mixture became transparent and then 10K MPEG-Silane (4 g) was immediately added to prevent capsule aggregation and stirred vigorously to disperse evenly. Within 5 min of the MPEG-Silane addition, anhydrous TEOS (30 ml) was added in one portion. The flask was sealed and the solution stirred vigorously at room temperature. After approximately 10 min, the flask was removed from the glovebox and stirred vigorously (about 1,000 rpm) at 65 °C under constant nitrogen pressure connected to a Schlenk line. A second portion of MPEG-Silane (4 g) was added after around 42 h. After about 48 h, the reaction crude was cooled to room temperature under constant nitrogen pressure, poured into a centrifuge tube and centrifuged at 8,670 × g (Fisher Lynx Sorvall centrifuge) for 1 h at room temperature (18-22 °C), after which the pellet was discarded. The supernatant was further centrifuged at 8,670 × g for 12–14 h at room temperature. After the second centrifuge, the paste-like UCNCs (approximately 8-10 g) were immediately transferred to the glovebox. See Fig. 3 and Extended Data Fig. 1 for representative characterization (scanning electron microscopy (SEM), transmission electron microscopy (TEM), photoluminescence, thermogravimetric analysis (TGA)). We have scaled this synthesis by 2-3× using the Vitamix blender with no apparent change in nanocapsule quality or physical/optical properties. Approximately half of the weight of the purified nanocapsule paste is composed of water, which later influenced the resin design. The paste must be dispersed in another solvent within a few days (for example, acrylic acid, water, acetone) before the water in the paste evaporates. UCNC paste dispersed in acrylic acid and stored in the dark for >24 h suggest good durability over time, as the upconversion photoluminescence remains constant compared with a freshly prepared sample. The thermal stability is also an important consideration, owing to the exothermic nature of chain-growth reactions in the 3D printing process. TGA of the UCNCs (Extended Data Fig. 1) shows that the decomposition onset temperatures of the UCNCs and each individual constituent are well above the expected printing temperatures (>200 °C for the sensitizer, annihilator and silane-terminated PEG).

## Measurements

Photographs were taken with a Canon EOS Rebel T6i, except where noted. The time-lapse videos were recorded with an iPhone 8 and/or an iPhone 12. All images presented are unedited.

Figure 1 images are of a dilute stock solution of PdTPTBP and BrTIPS-anthracene. The quadratic voxel was generated with 637-nm light. The linear voxel was generated from a fibre-coupled 365-nm LED coupled into the same optical path. The contents in the linear cuvette were diluted by a factor of two relative to the contents in the quadratic cuvette to better show the entire voxel. The spot size was measured by moving a razor blade through the spot with a micrometer. The excitation sources are focused through a 50× objective with a 0.55 NA.

Figure 3b and Extended Data Fig. 1g images are taken with the same camera with the sample excited in free space by a 635-nm laser from the right through a 550-nm short-pass filter. In Extended Data Fig. 1g, capsules and F127 micelles<sup>24</sup> were diluted 30:1 in the specified solvent. The tap water was taken directly from the sink and left uncapped for 20 min before the image was taken. All other samples were prepared in the glovebox.

For Fig. 3d, the UCNCs and micelles (oleic acid nanodroplets stabilized by APTES but without TEOS and MPEG-Silane) were diluted 100:1 in the specified solvent. The upconversion photoluminescence spectra presented in Fig. 3d has the laser scatter omitted (around 635 nm).

 $Absorption\, spectra\, were\, collected\, on\, a\, Cary\, 5000\, UV-Vis\, spectrometer.$ 

Photoluminescence spectra were recorded with an Ocean Optics QE Pro. For the intensity dependence presented in Fig. 2, the incident laser intensity was measured with a calibrated Si photodetector from Newport and varied using neutral-density filters. The emission intensity was measured with the QE Pro spectrometer and integrated. No variation in emission shape or time was observed throughout the measurement.

The SEM image presented in Fig. 3 was captured by using an in-lens (immersion lens) detector on a Supra55VP Field Emission Scanning Electron Microscope (FESEM) at  $10\ \text{keV}$ . Capsule paste dispersed in water was drop-cast on the sample mount.

The TEM image presented in Extended Data Fig. 1 was captured by a JEOL-2100 high-resolution transmission electron microscope operated at 200 kV. Capsule paste dispersed in water was drop-cast on a polymer-coated Cu grid.

TGA presented in Extended Data Fig. 1 was performed using a TA Instruments TGA Q500 with high-resolution sensitivity at a ramp rate of  $50 \,^{\circ}$ C min<sup>-1</sup> with  $4.00 \,^{\circ}$ C resolution under nitrogen flow up to  $1,000 \,^{\circ}$ C.

Dynamic light scattering presented in Extended Data Table 1 was collected on a Brookhaven Instruments 90Plus Nanoparticle Size Analyzer. The temperature was fixed at 25 °C with a 5-s equilibration time and three total measurements. A sample of the supernatant was collected after the first centrifuge step during purification, diluted  $10\times$  in Milli-Q water and filtered with a 0.2  $\mu m$  polyvinylidene difluoride (PVDF) syringe filter into a 1-cm polystyrene cuvette. Nanoparticle aggregation was not observed when analysing samples with an order of magnitude difference in concentration.

A Thorlabs Power Meter PM100D with a S120VC photodiode was used to measure the voxel power as a function of the laser dial setting as used on the FDM printer and the focal plane power as used on the DMD printer.

Images presented in Fig. 4i, j were taken with an inverted microscope (Nikon Eclipse Ti2) with a  $4 \times$  magnification illuminated with a red lamp. The images were collected with a Kiralux 8.9 MP Color CMOS Camera purchased from Thorlabs.

The image presented in Extended Data Fig. 3g was taken with an inverted microscope (Nikon Eclipse Ti2) with a  $4 \times$  magnification illuminated under white light. The image was collected with a Kiralux 8.9 MP Color CMOS Camera purchased from Thorlabs.

## Monovoxel excitation using the FDM printer

**Br-TIPS-anthracene resin preparation (10 ml resin).** All resins were prepared in a nitrogen atmosphere under red light in a 20-ml scintillation vial covered in aluminium foil. To 150 mg of Aerosil 200 silica, 5 ml PETA was added and the mixture was stirred at 90 °C for 15 min, and then

the temperature was reduced to 60 °C and the solution was allowed to cool for 30 min. To the hot PETA/Aerosil 200 solution, TEMPO (30 ul of a freshly prepared 1 mg ml<sup>-1</sup> acrylic acid solution diluted from 10 mg ml<sup>-1</sup>) and Sudan I (40 µl of a freshly prepared 1 mg ml<sup>-1</sup> acrylic acid solution diluted from 10 mg ml<sup>-1</sup>) were added. The solution was inverted to mix before adding Ivocerin (550 mg) and 500 µl acrylic acid. The solution was stirred at 60 °C for 30-45 min, to ensure that it was optically transparent. Then, the capsule paste solution (2.5 ml of a 0.67 g ml<sup>-1</sup> solution in acrylic acid, stirred for >1 h at room temperature) and acrylic acid (1 ml) were added. A polar protic monomer was required to disperse the UCNCs, owing to the moderate water content of the capsule paste and polar PEG chains affixed to the nanocapsule surface. After shaking the resin, PETA was added for a total resin volume of 10 ml. The solution was then sparged under nitrogen for 15 min at 60 °C. The resin was allowed to stir and cool to room temperature on the warm hotplate for 1 h. The resin was then poured into a polystyrene cuvette (3.5 ml, 1-cm path length, sealed with Parafilm), mixed in a FlackTek SpeedMixer to remove bubbles (1,000 rpm, 5-8 min) and used immediately for printing. The final optimized resin contains about 15 wt% UCNCs. We affirm that the high UCNC loading does not appreciably affect the ability to print deep within a vat, as the optimized resin transmits >85% of 637-nm light through a 1-cm polystyrene cuvette. During the TEMPO concentration optimization, we found that, at constant printing power, the TEMPO concentration is directly proportional to the print speed required for comparable prints. Ultimately, we find that the concentrations of Ivocerin, TEMPO and Sudan I can be fine-tuned, depending on the desired print power, speed and resolution, with the optimized resin presented herein allowing for rapid printing and sharp features.

**Printing.** The printing is performed on a custom-built, highly modified Kossel Delta configuration RepRap printer, with many modifications gathered from Haydn Huntley (https://www.kosselplus.com/) (Extended Data Fig. 2). The firmware run on the printer is a fork of RepRap (RepRapFirmware-dc42, available at https://github.com/dc42/RepRapFirmware) and the printing electronics are the Duet 2 Wifi controller (https://www.duet3d.com/DuetWifi). Standard Tessellation Language (STL) files are sliced in Simplify3D to generate gcode inputs to the printer. The Benchy code parameter (STL, gcode) files are provided in Supplementary Data 1 and 2.

The printing is powered by a Thorlabs S4FC637 637-nm 70-mW fibre-coupled laser (Extended Data Fig. 2). The laser is collimated with a 20-mm-focal-length lens and then fed into a 50× Mitutoyo Plan Apochromat Objective, where it is focused into the resin. The entire optical system is moved by the printer in three dimensions to generate the print. Benchy is printed from the bottom of the cuvette to the top (Supplementary Video 2). The print starts at a laser power setting of 16–17 mW. The laser power setting is reduced to 15–16 mW after 1 h. The optical throughput is about 25%, leading to a measured output power of <4 mW at the focal point; we measure power to be between 3.6 and 3.9 mW, and power densities of  $4.5 \times 10^3 - 4.9 \times 10^3$  W cm<sup>-2</sup>, on the basis of a 10.1-µm measured diameter of the focal point. The print is run at a speed of 50% relative to the speed outlined in the gcode file for a total time of 1 h 50 min (Supplementary Data 1 and 2). After printing, the final part was washed in 2:1 tri(propylene glycol) methyl ether/5% acetic acid ( $3 \times 60$  ml) to remove unreacted resin and allowed to dry at room temperature in an ambient atmosphere in the dark. Control resins did not print within the power range and time required for printing (resins without UCNCs or resins with UCNCs but without a photoinitiator).

## Parallel excitation using the DMD printer

**TIPS-anthracene resin preparation (10 ml).** The resin preparation is identical to that of the Br-TIPS-anthracene resin with the following edits.

First, after sparging the resin under nitrogen, the resin was allowed to stir at 45 °C instead of at room temperature.

Second, for the gear and the Stanford University logo (Fig. 4g, h), instead of pouring the resin into a cuvette, about 0.5 ml of resin was poured into a 35  $\times$  10-mm Falcon brand polystyrene Petri dish and well sealed with Parafilm. Pouring a thin layer of the resin into the high-surface-area Petri dish removed bubbles adequately, as long as the resin was stirred at 45 °C after the nitrogen sparge, eliminating the need for the FlackTek SpeedMixer.

Third, for lines (Fig. 4i), when printing very small features with light projected through a mask, it was vital to minimize the distance between the top of the mask and the resin. Instead of using a Petri dish, a few drops of resin were sealed into a box constructed from 1-in² glass microscope slide coverslips. To protect the resin from oxygen, the box was constructed the day before, leaving the top open. The edges were sealed with epoxy and cured under ultraviolet light. Then, when used for printing, the top was sealed with a small piece of polystyrene plastic and epoxy. At this stage, the epoxy could not be cured, as this would also cure the resin inside the box. However, this seal was sufficient to print immediately after removing the resin from the glovebox.

The printing is performed on a custom-built setup as described below. The two-dimensional printing is performed using a custom-built DMD projection, as shown in Extended Data Fig. 2 and Supplementary Video 4. The DMD hardware is from Texas Instruments (DLP Light-Crafter 6500 Evaluation Module (DLPLCR6500EVM)). The software used to control the DMD is the Texas Instruments DLP LightCrafter 6500-4.0.1 graphical user interface. Patterns are projected by uploading monochromatic bitmap images using 'pattern-on-the-fly' mode. To project the displayed pattern onto the resin, the DMD is illuminated using a Luminus Devices CBT-90 Red R5 LED focused using a Thorlabs AL5040M to uniformly illuminate the display area of the DMD. The CBT-90 is driven by a Xantrex (now Ametek/Sorensen) HPD 15-20 current/ voltage source and is mounted on a PhlatLight heat sink. The illuminated pattern is reflected from the DMD to a Thorlabs PF20-03-P01 mirror, which reflects the pattern through a Thorlabs LA1433-B. This focused image is then reflected off a Thorlabs PF20-03-P01 mirror and through a Thorlabs AC508-100-A-ML lens, which projects the image onto the resin at the focal point of the lens.

We could not generate a print with an UCNC-free control resin nor with a Br-TIPS-anthracene-based resin, owing to the high upconversion threshold, further highlighting the importance of matching the appropriate threshold upconversion system to a specific printing motif.

The images of the gear and Stanford University logo (Fig. 4g, h) projected by the DMD were printed in 8 min at a power density of 78 mW cm $^{-2}$ . After printing, the final part was washed in 2:1 tri(propylene glycol) methyl ether/5% acetic acid (3 × 60 ml) to remove unreacted resin and allowed to dry at room temperature in an ambient atmosphere in the dark.

The lines printed in Fig. 4i were printed in 17 s at a power density of 224 mW cm<sup>-2</sup> using light projected by the DMD through the Negative 1951 United States Air Force Wheel Pattern Resolution Test Targets,  $3'' \times 1''$  (Thorlabs).

## **Data availability**

The data supporting this study are available from the corresponding author on reasonable request.

## **Code availability**

The code used in this manuscript is supplied in Supplementary Data 1 and 2.

Acknowledgements S.N.S. acknowledges the support of the Arnold O. Beckman Postdoctoral Fellowship. M.S. acknowledges financial support through a Doc. Mobility Fellowship from the Swiss National Science Foundation (project no. P1SKP2 187676). A.O.G. acknowledges the support of a National Science Foundation Graduate Research Fellowship under grant DGE-1656518 and a Stanford Graduate Fellowship in Science & Engineering (SGF) as a Scott A. and Geraldine D. Macomber Fellow. We thank C. J. Brinker from the University of New Mexico and S. Kommera from Stanford University for their helpful discussions, V. A. Lifton from Evonik for supplying the Aerosil 200, and A. Sellinger and A. Lim from Colorado School of Mines for performing the TGA experiments. This research is financed through the support of the Rowland Fellowship at the Rowland Institute at Harvard University, the Harvard PSF Accelerator Fund and the Gordon and Betty Moore Foundation. Portions of this work were performed at: the Harvard Center for Nanoscale Systems (CNS), a member of the National Nanotechnology Coordinated Infrastructure Network (NNCI), which is supported by the National Science Foundation under NSF award no. 1541959: the Stanford Nano Shared Facilities (SNSF), supported by the National Science Foundation under award ECCS-2026822; the Stanford ChEM-H Macromolecular Structure Knowledge Center. The STL file for 3DBenchy - The jolly 3D printing torture-test by CreativeTools.se by CreativeTools is licensed under the Creative Commons - Attribution - No Derivatives license. The image of the gear we present in Fig. 4 and Extended Data Fig. 2 was reproduced with permission from Alamy Inc./Natalia

Author contributions D.N.C. and S.N.S. conceived the project. S.N.S., D.A., M.K.G. and T.H.S. developed the UCNCs. M.K.G. conducted the microscopy characterization of UCNCs. D.N.C., S.N.S. and T.H.S. developed the 3D printing resins. D.N.C., M.S., A.O.G. and R.C.S. constructed the 3D printers and optical setups. T.H.S. and A.O.G. generated the parts presented in this manuscript. D.N.C. directed the project.

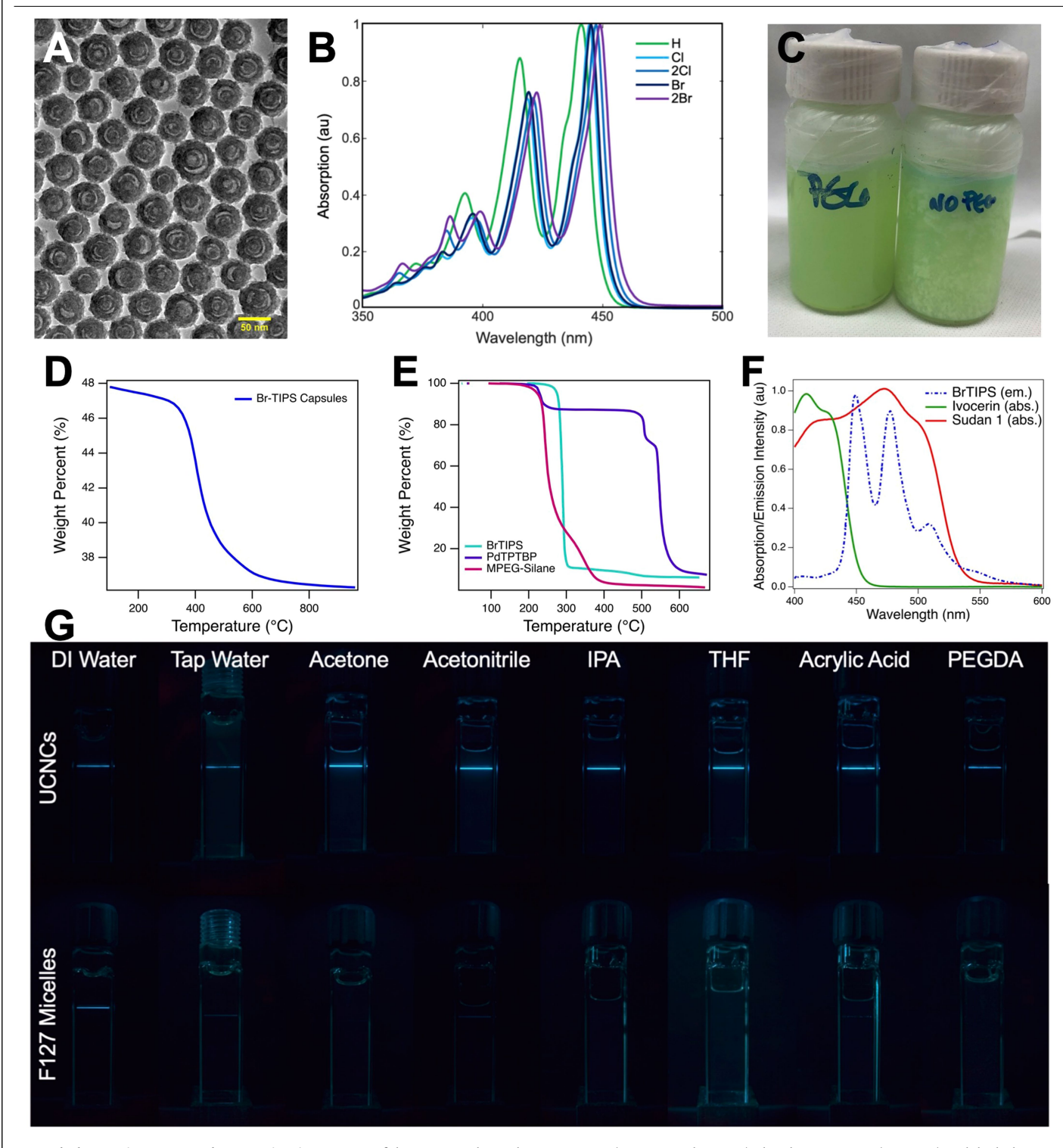
Competing interests Harvard University has filed several patents on the basis of this work. S.N.S., R.C.S. and D.N.C. are co-founders of Quadratic3D, Inc. S.N.S. is the Chief Technological Officer, D.N.C. is the Chief Scientific Advisor and R.C.S. is an advisor to Quadratic3D, Inc.

#### Additional information

Supplementary information The online version contains supplementary material available at https://doi.org/10.1038/s41586-022-04485-8.

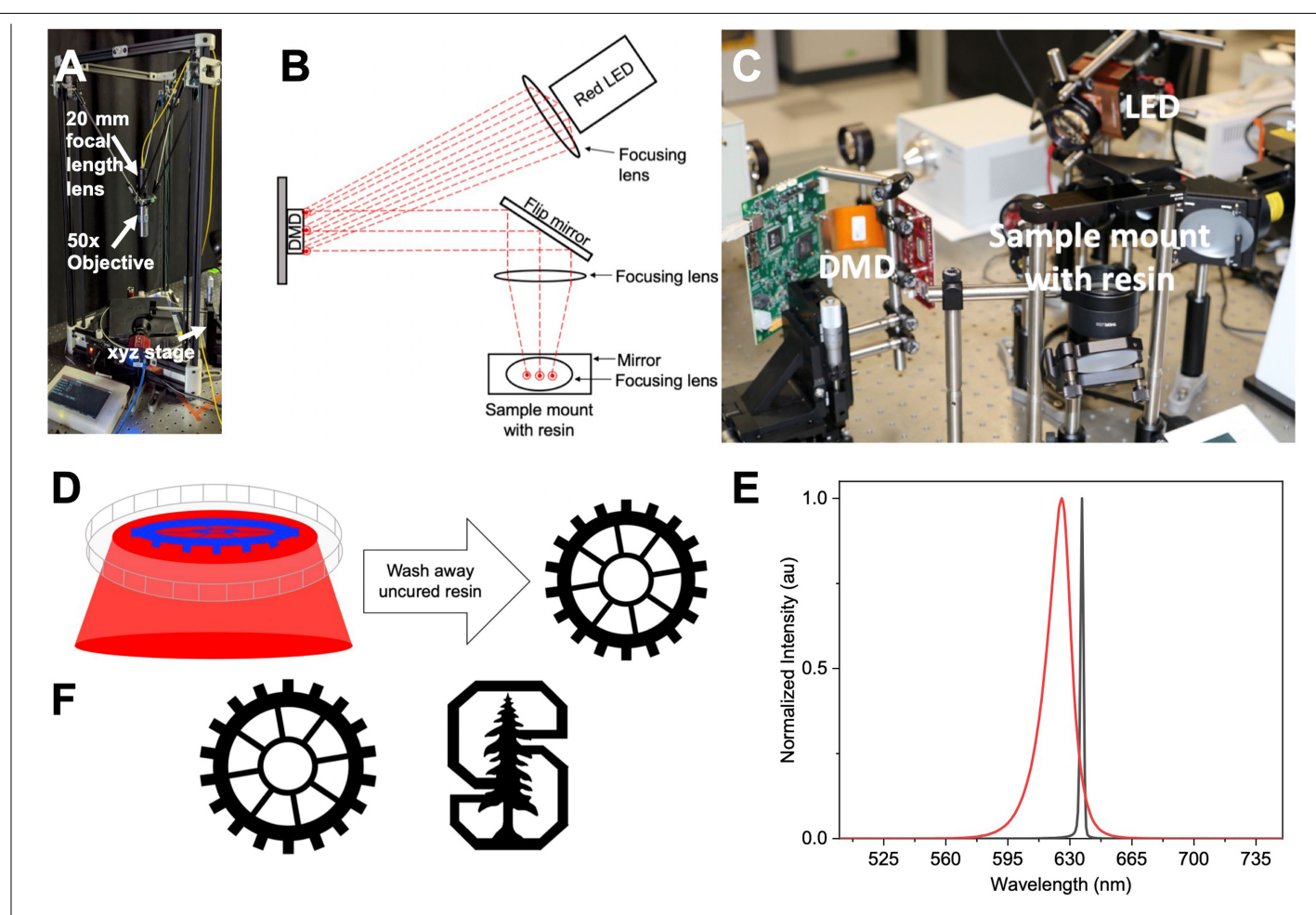
**Correspondence and requests for materials** should be addressed to Daniel N. Congreve. **Peer review information** *Nature* thanks Christophe Moser and the other, anonymous, reviewer(s) for their contribution to the peer review of this work.

Reprints and permissions information is available at http://www.nature.com/reprints.



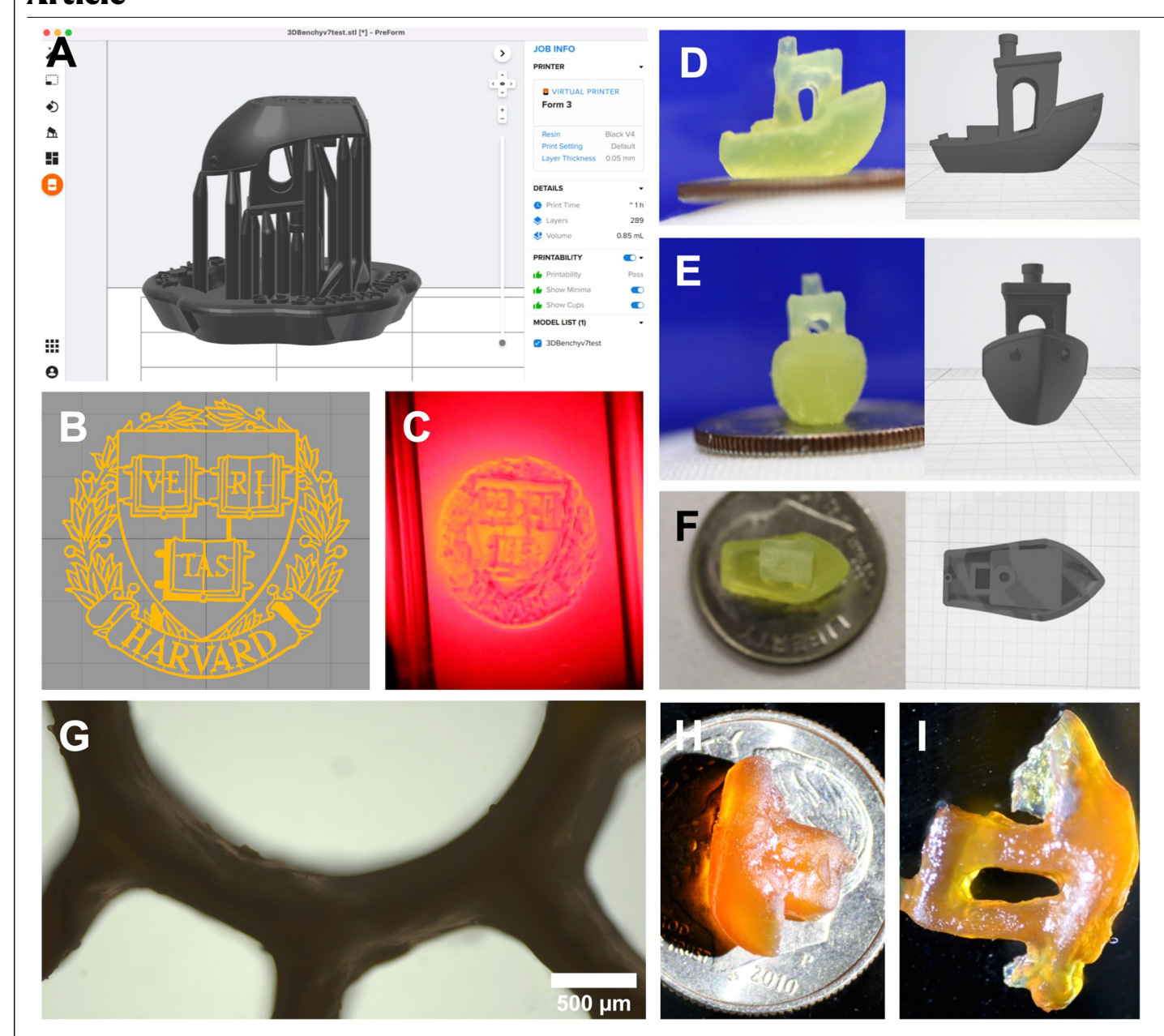
**Extended Data Fig. 1** | **UCNC characterization. a**, TEM of the UCNCs. The scale bar represents a length of 50 nm. **b**, Absorption spectra of the annihilators used in this work. **c**, Photograph of UCNCs dispersed in water with and without the addition of MPEG-Silane. A precipitate rapidly forms (<1 h) in the vial without MPEG-silane, probably owing to nanocapsule aggregation. This aggregation is irreversible. TGA of capsule paste (**d**) and capsule constituents in nitrogen (**e**). In panel **d**, the temperature was held at 100 °C until the capsule paste mass remained constant. **f**, Emission–absorption overlap between the upconverted

emission (Br-TIPS-anthracene), the photoinitiator (Ivocerin) and the light blocker (Sudan I).  ${\bf g}$ , UCNCs and F127 micelles  $^{24}$  dispersed in various solvents. UCNCs and F127 micelles were both synthesized in water and added at a 1:30 ratio to the listed solvents. They were then excited at 635 nm and imaged through a 550-nm short-pass filter. The tap-water sample was dispersed in water directly from the tap and left uncapped for 20 min before taking the image. Acrylic acid and PEGDA were each used to assess capsule durability in acrylate-based monomers for printing resins.



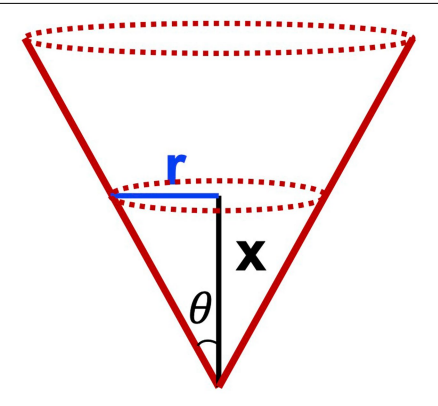
**Extended Data Fig. 2** | **Printing schematics. a**, Photograph of the FDM printing setup, which moves a laser spot in three dimensions. The original instructions for the FDM printer are found at https://www.kosselplus.com/, with our modifications presented above. Cartoon schematic ( $\mathbf{b}$ ) and photograph ( $\mathbf{c}$ ) of the DMD printing system, which allows for stationary, parallel excitation at one time.  $\mathbf{d}$ , Cartoon depiction of the UCNC-facilitated

printing process using parallel excitation.  $\mathbf{e}$ , Emission spectra of the light sources used to generate prints (black: 637-nm fibre-coupled laser for the monovoxel excitation printer; red: 625-nm LED for the parallel excitation printer).  $\mathbf{f}$ , The file images projected by the DMD to print the Stanford University logo and gear presented in the main text.



Extended Data Fig. 3 | 3D printing with UCNCs. a, Formlabs print simulation of the same Benchy STL. The file was imported into the free software PreForm 3.18.0 and simulated for printing on a Form 3B printer at 50-μm layer height. The boat was scaled to match the dimensions of the Benchy printed on our printer. The boat, without support structures, required 200 layers and 0.14 ml of resin. At this point, we used the 'one-click-print' function to generate the printable structure with support structure. This resulted in an object with 289 layers at 50-μm layer height, using 0.85 ml of resin. The STL file image (b) and a photograph (c) of the Harvard University logo presented in Supplementary Video 3. The Harvard University logo presented here was printed using a different resin formulation with bis(5·2,4-cylcopentadien-1-yl)-bis(2,6-difluoro-3-(1H-pyrrol-1-yl)-phenyl) titanium (titanocene, Gelest) as a photoinitiator instead of Ivocerin. This resin was prepared with 1.9 wt% Aerosil 200, 3 wt% titanocene, 13 wt% Br-TIPS-anthracene capsules, 0.03 wt%

Sudan I and 5 ppm TEMPO. This resin formulation limited printing resolution, hence the emphasis on the use of the resin presented in the main text and Methods.  $\mathbf{d}$ – $\mathbf{f}$ Side-by-side comparisons of the STL file schematic to the corresponding Benchy photograph from the same perspective. The boats presented in panels d-f were printed using the resin formulation described in the Methods section.  $\mathbf{g}$ , A representative image of a gear under the microscope shows that round and straight features are generally smooth. The images were taken after washing away excess resin and allowing the gear to dry under an ambient atmosphere in the dark.  $\mathbf{h}$ , An overprinted boat gives a lack of discernable features.  $\mathbf{i}$ , An underprinted boat shows missing features and damage from the wash process. Both issues are remedied by altering the print speed and irradiation power. The boats presented here were printed using the same resin formulation as the Harvard University logo presented in panel  $\mathbf{c}$ .



Input light focused by the 0.55 NA objective used for monovoxel-based printing

r: Radius of the voxel cross section at the quadratic threshold

x : Distance from the focal point where printing occurs in the quadratic regime

1) Determine the area (A) of the voxel cross section at the quadratic threshold for BrTIPS-Anthracene. The 4 mW is the measured power (P) at the focal point, as reported in the monovoxel printing methods section, and the 121,100 mW cm<sup>-2</sup> ( $I_{th}$ ) is the quadratic threshold presented in Fig. 2.

$$A = \frac{P}{I_{th}} = 4 \, mW * \frac{1 \, cm^2}{121,100 \, mW} * \frac{(10^4 \, \mu m)^2}{(1 \, cm)^2} = 3,300 \, \mu m^2$$

2) Determine the radius (r) of the voxel cross section at the quadratic threshold (Fig. 2) for BrTIPS-Anthracene.

$$A = \pi r^2$$

$$3,300 \mu m^2 = \pi r^2$$

$$r = 32.4 \mu m$$

3) Determine the angle ( $\theta$ ) using a 0.55 NA objective and an index of refraction (n) of ~1.5 for the resin.

$$NA = n \sin(\theta)$$
$$0.55 = 1.5 \sin(\theta)$$
$$\theta = 21.5^{\circ}$$

4) Determine the distance from the focal point that printing occurs in the quadratic regime based on the radius of the voxel cross section determined in (2).

$$x = (32.4 \,\mu m) \cot(21.5^{\circ})$$

$$x = 82 \, \mu m$$

**Extended Data Fig. 4** | **Printing in the quadratic regime.** The *z* distance from the focal point of the voxel in which the printing in the quadratic regime is approximated. We assume an approximately constant illumination profile.

# Upconverted Light

# Photoinitiation in Resin

 $\label{lem:converted} \textbf{Extended Data Fig. 5} | \textbf{Printing resolution note 1: blurring of the upconverted voxel in the printing resin.} \textbf{Cartoon depiction (not to scale) of the blurring that occurs between the shape of the upconverted voxel and the photoinitiation in resin caused by absorption of the upconverted light. Although upconverted light generates light in nanocapsules that emits$ 

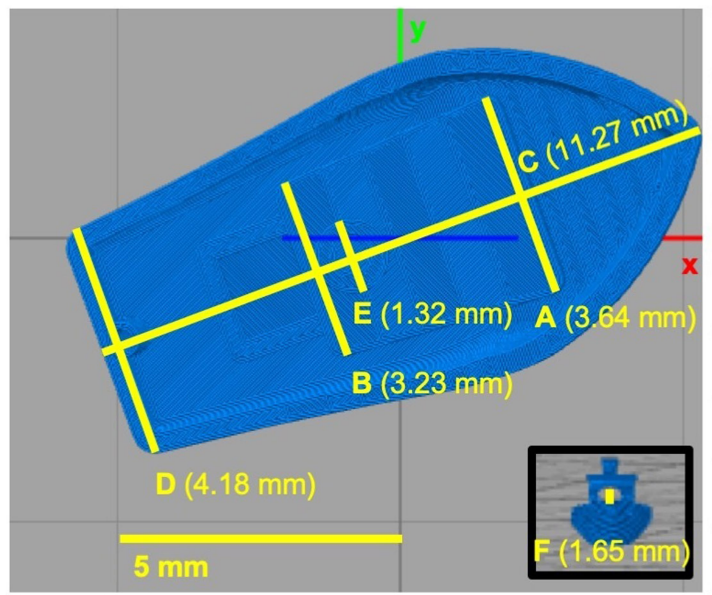
isotropically from a focal point, this light must subsequently be absorbed by the photoinitiator to cause polymerization. This emission and reabsorption introduce a blurring function to the print that is dependent on the Beer–Lambert law for the distance that the light travels before reabsorption.

## Extended Data Table 1 | Dynamic light scattering

Entry	Effective Diameter (nm)	PDI	Diffusion Coefficient (x 10 <sup>-8</sup> cm <sup>2</sup> s <sup>-1</sup> )	Data Retained (%)
1	76.82	0.12	6.39	99.49
2	76.09	0.16	6.45	98.16
3	77.34	0.14	6.35	99.08

Summary of dynamic light-scattering characterization of UCNCs. Each entry represents an average of three measurements from different batches of UCNCs synthesized on the scale presented in the Methods. This summary highlights the reproducibility of this synthesis on the multi-gram scale.

## Extended Data Table 2 | Benchy comparison with STL dimensions



	Length (mm)			
	STL dimensions	Benchy 1	Benchy 2	
Α	3.64	3.88	3.57	
В	3.23	3.51	3.19	
C	11.27	11.34	11.82	
D	4.18	4.22	4.26	
Ε	1.32	1.16	1.12	
F	1.65	1.37	1.39	

A comparison between the projected STL dimensions and the measured dimensions on two unique Benchy boats, as measured with calipers.

## Extended Data Table 3 | Resolution test line width quantification

	Column 1	Column 2	Column 3	Column 4
Actual Width (μm)	65.00	55.00	50.00	45.00
Average Printed (µm)	74.35	62.68	55.30	49.51
Std. Dev (μm)	7.99	5.10	3.95	4.84
Std. Dev (μm)	7.99	5.10	3.95	4.8

The quantification of the line widths of the print presented in Fig. 4i. The width of each line was measured in 2–3 places, for a total 18 measurements averaged for lines in columns 1–3. The width of each line was measured in 1–3 places, for a total of ten measurements averaged for lines in column 4.

Extended Data Table 4 | Printing resolution note 2: the light path length as a function of photoinitiator concentration and molar absorptivity at  $450 \, \text{nm} \, (A = \varepsilon cl)$ 

Entry	Transmission (%)	Absorbance, A (a.u.)	Molar Absorptivity, ε (L mol <sup>-1</sup> cm <sup>-1</sup> )	Path Length, l (cm)	Concentration, c (mol L <sup>-1</sup> )
1	10	1	100	0.071	0.14
2	10	1	1000	0.0071	0.14
3	10	1	10000	0.00071	0.14

We can improve the resolution by exchanging the photoinitiator system with a system that confines light to a small path length more efficiently. Take our use of Ivocerin, which has a molar absorptivity of 100 L mol<sup>-1</sup> cm<sup>-1</sup> at 450 nm (reference: data sheet from our supplier, Synthon), where there is marked spectral overlap with the upconversion emission. According to Beer's law, at a concentration (c) of 0.14M (Methods), this translates to a path length (l), or 'light confinement', of roughly 700 microns (0.071 cm) for 90% of the light or, conversely, 10% of light will transmit further than this path length (entry 1). As the molar absorptivity of the photoinitiator increases, the light is confined to smaller and smaller path lengths at a constant photoinitiator loading (entries 1–3). Although Beer's law assumes a linear light path, similar improvements can be found in this geometry. Considering the voxel as roughly ellipsoidal in shape and not an infinitesimally small point, upconverted light originating not only from the centre of the voxel but also the outer edges of the voxel contribute to non-trivial blurring of the upconverted light to the as-printed, photoinitiated voxel. Thus, at this time, the most crucial resolution limitation is light confinement. Although this can be managed with the use of optical absorbers and carbon-carbon radical inhibitors (Sudan I and TEMPO, respectively), it cannot be completely overcome by chemical means alone. This poor light confinement can be remedied by improving the spectral overlap of the upconversion emission with Ivocerin, by exchanging Ivocerin for a new photoinitiator with a higher molar absorptivity at the maximum upconversion emission, or a combination of both strategies. Taken together, future efforts will seek to improve the energy transfer from the UCNCs to the photoinitiator for increased resolution.

## $\textbf{Extended Data Table 5} \,|\, \textbf{Upconversion photopolymerization}$

Upconverting Materials	Excitation wavelength	Excitation Power/ Power density	Printing Details
NaYF <sub>4</sub> : Yb,Tm nanoparticles	980 nm	90 W cm <sup>-2</sup>	Then the samples were molded in cylinders (Ø1 mm) of different thicknesses (1–10 mm). Finally, the premixed and molded specimens were exposed to a NIR laser ( $\lambda$ = 980 ± 5 mm, continuous wave, CNI, China) for intervals from 30 s to 5 min. Composite samples of 5 mm thickness were cured two times faster than pure polymer cured by blue light (30 and 60 s, respectively). (max 7-10 mm). Ref. <sup>34</sup>
NaYF4:18%Yb,0.5%Tm nanoparticles	980 nm	9.4 W cm <sup>-2</sup>	The photocurable samples were injected into a glass tube (17.78 cm long with an outer radius of 5 mm and an inner radius of 4 mm), and then the glass tube was vertically exposed to a fiber coupled laser system (980 nm, Changchun New Industries Optoelectronics Technology). The output power was adjusted to 7.4 W for the activation of the UCNPs. After 2 min irradiation, the cured samples were transferred out of the tube and the uncured parts were washed away by acetone. Ref. <sup>35</sup>
Tm³+ doped K₂YbF₅ nanoparticles	980 nm	0.3 W	A suspension of micrometer-sized up-converting 0.2 at% Tm³-doped K <sub>2</sub> YbF <sub>5</sub> and a liquid PEGDA resin containing 1.0% in weight of UV-sensitive Irgacure-819® has been prepared in a proportion of 100 g L⁻¹. Then, the laser diode describes a previously designed pattern, controlled with an X-Y axis micrometer positioner, even with a continuous moving over the liquid surface (at an estimated speed of 0.3 mm s⁻¹) in order to provide local polymerization of the resin. Ref. <sup>36</sup>
NaYF4: Er@NaYF4 nanoparticles	1550 nm	See print image	20 μL of NaErF <sub>4</sub> @NaYF <sub>4</sub> nanoparticles in ethanol dispersion (0.01 M) was first drop-casted on the microring-resonator. After the ethanol was evaporated, a 2 μm thick SU-8 2002 was spin-coated on the device followed by baking at 90 °C for 10 min. The device was then placed on an alignment stage to align the input/output fiber array with the device. To align the evavelength and polarization of the laser with the microring resonator, we first use a very low inlaser power and slowly tune the wavelength as well as adjust the polarization controller until power at the drop port is maximized. Using a very low laser power for finding the resonance wavelength was to avoid too much light exposure to the straight bus waveguide and microring resonator at this stage. Once the resonance and polarization are aligned between the input and the resonator, the laser was then increased to 20 μW to start the curing process. After 10 min the device was removed from the alignment stage and transfer of a 90 °C hoplate for 10 min of post exposure bake procedure. After the device was cooled down to room temperature, then remove the unexposed part of SU-8 by immersing the device into the SU-8 developer for 1 min and finally rinsed in water. Ref. <sup>37</sup>
NaYF <sub>4</sub> :Yb <sup>3+</sup> ,Tm <sup>3+</sup> /NaYF <sub>4</sub> nanoparticles	975 nm	7 W cm <sup>-2</sup>	Commercial CW laser diode at 975 nm (ATC-SD, Russia) was focused by an objective in PCC volume, containing UCNPs. The power density of the laser was set at 15 W cm <sup>-2</sup> . As a proof of feasibility of the proposed approach for creation of the 3D printed device macroarchitecture, the hollow tube formation with the diameter of 1.5 mm and the height of 2 mm was obtained by layer-by-layer drawing directly in the resin volume. The PCC was scanned by the laser via 2-axis galvano-scanner Miniscan-07 (Raylase, Germany). The displacement of voxel along the z-axis was carried out by a micrometric translation stage (Thorlabs). After finishing of the drawing process, the tube was removed and developed in 2-propanol. Ref. <sup>38</sup>
β-phase NaYF <sub>4</sub> :TmYb@NaYF <sub>4</sub>	974 nm	0.64 W cm <sup>-2</sup>	For the patterning of proteins, a photomask was positioned between the NIR light and the proteins. In the exposed areas, UCNPs convert NIR light into blue light that induces cleavage of the Ru complexes and the local release of proteins. The Ru-UCNP substrate was irradiated with 974-nm light (0.64 W/cm²) for 40 minutes. Ref. 39
NaYF <sub>4</sub> : Yb <sup>3+</sup> , Tm <sup>3+</sup> nanoparticles	980 nm	3-6 W	The UV-curable composition was placed in a cavity inside a glass panel. The sample containing acrylate monomer, photo-initiator (PI) and UCPs was exposed to NIR radiation cum disparate intensity. Ref. 40
βNaYF4:18%Yb,0.5%Tm nanoparticles	980 nm	19.3 W	The formulation contained 0.3 wt % of UCNPs, 0.3 wt % of photoinitiator Irgacure 784, and equal molar ratio of thiol-ene. The photosensitive resin was injected into a glass tube, which was then vertically exposed to a 980 nm laser. The output power of the laser and the exposure time were 19.3 W and 40 s, respectively. The cured samples were transferred out of the tube and the uncured parts were washed away with acetone. Ref. 41
β-NaYF <sub>4</sub> :Yb <sup>3+</sup> , Tm <sup>3+</sup> nanoparticles	975 nm	~ 100 W/cm <sup>2</sup>	A mixure of oligocarbonate methacrylate (OCM-2), photoinitiator Irgacure 369, and nanoparticles was used as the photocurable composition for the UCNP-assisted NIR polymerization in bulk. First, 10 mg of Irgacure 369 was mixed with 1 g OCM-2, then, 100 µL UCNP dispersed in hexane (c = 0.2 g/mL) was added and the mixture was thoroughly shaken and sonicated until the hexane evaporated. The photopolymerization occurred in a laser beam (975 nm) focused into a specific volume of glass vial containing the photocurable composition at a laser power of ~ 100 W/cm² for 20 s. Ref. 42
TTA-upconversion system: IBDP-IBDP and perylene in nanomicelles	635 nm	4.6 mW	Photopolymerization system: monomer: 2-hydroxylethyl acrylate (HEA); photoinitiator: Irgacure 784, irradiated with 635 nm cw laser (2 mW, power density at a focal point is 0.26 W cm <sup>-2</sup> ) irradiation for 40 s. For each measurement, Irgacure 784 (2 mg) was added into 0.5 mL HEA (heating with dryer to fully solubilized it), then nanomicelle mother solution (0.5 mL) was added. The mixture was filtered out by Syringe-driven Filter (Nylon, 0.22 µm) to obtain the clear and transparent nanomicelle photopolymerization solution for measurement. Ref. <sup>43</sup>

 $Recent\ examples\ of\ upconversion-facilitated\ photopolymerization.$